REPORT DOCUMENTATION PAGE

Form Approved
OMB No. 0704-0188

1. REPORT DATE *(DD-MM-YYYY)*	2. REPORT TYPE	3. DATES COVERED *(From - To)*
14 April 2003	Technical Paper	

4. TITLE AND SUBTITLE

Evidence of Collisionless Shocks in a Hall Thruster Plume

5a. CONTRACT NUMBER

5b. GRANT NUMBER

5c. PROGRAM ELEMENT NUMBER

6. AUTHOR(S)

Brian E. Beal, Alec D. Gallimore, William A. Hargas

5d. PROJECT NUMBER
1011

5e. TASK NUMBER
0011

5f. WORK UNIT NUMBER

7. PERFORMING ORGANIZATION NAME(S) AND ADDRESS(ES)

The University of Michigan
Plasmadynamics and Electric Propulsion Laboratory
Department of Aerospace Engineering
Ann Arbor, MI 48109

8. PERFORMING ORGANIZATION REPORT NUMBER

AFRL-PR-ED-TP-2003-102

9. SPONSORING / MONITORING AGENCY NAME(S) AND ADDRESS(ES)

Air Force Research Laboratory (AFMC)
AFRL/PRS
5 Pollux Drive
Edwards AFB CA 93524-7048

10. SPONSOR/MONITOR'S ACRONYM(S)

11. SPONSOR/MONITOR'S NUMBER(S)
AFRL-PR-ED-TP-2003-102

12. DISTRIBUTION / AVAILABILITY STATEMENT

Approved for public release; distribution unlimited.

13. SUPPLEMENTARY NOTES

14. ABSTRACT

15. SUBJECT TERMS

16. SECURITY CLASSIFICATION OF:			17. LIMITATION OF ABSTRACT	18. NUMBER OF PAGES	19a. NAME OF RESPONSIBLE PERSON
					Sheila Benner
a. REPORT	b. ABSTRACT	c. THIS PAGE	A		19b. TELEPHONE NUMBER *(include area code)*
Unclassified	Unclassified	Unclassified			(661) 275-5693

FILE

MEMORANDUM FOR PRS (In-House Publication)

FROM: PROI (STINFO) 25 Apr 2003

SUBJECT: Authorization for Release of Technical Information, Control Number: **AFRL-PR-ED-TP-2003-102**
Brian E. Beal & Alec D. Gallimore (Univ of MI); William A. Hargus (AFRL/PRSS), "Evidence of Collisionless Shocks in a Hall Thruster Plume"

Journal Article – Physics of Plasmas **(Statement A)**
(Deadline: 14 May 2003)

Evidence of collisionless shocks in a Hall thruster plume

Brian E. Beal and Alec D. Gallimore

Plasmadynamics and Electric Propulsion Laboratory, Department of Aerospace Engineering, The University of Michigan, College of Engineering, Ann Arbor, Michigan 48109

William A. Hargus, Jr.

Air Force Research Laboratories, Edwards Air Force Base, Edwards, California 93524

Triple Langmuir probes and emissive probes are used to measure the electron number density, electron temperature, and plasma potential downstream of a low-power Hall thruster. The results show a high density plasma core with elevated electron temperature and plasma potential along the thruster centerline. These properties are believed to be due to collisionless shocks formed as a result of the ion/ion acoustic instability. A simple model is presented that shows the existence of a collisionless shock to be consistent with the observed phenomena.

I. INTRODUCTION

Future Unites States Air Force (USAF) plans foresee a need for electric propulsion systems capable of operating at very high power levels compared to those currently in use. [1,2] One method being considered for reaching these power levels involves clustering multiple moderately-powered Hall thrusters together to reach the total throughput desired. In an effort to understand the technical issues related to operating multiple Hall thrusters in close proximity to each other, a cluster of four Busek BHT-200-X3 200-watt class devices is being studied both at the Air Force Research Laboratory (AFRL) and at the University of Michigan.[3-5] Since this particular thruster is pivotal to programs of near term interest, a comprehensive effort to study the plume properties of this device has been undertaken.

The plasma density, electron temperature, and plasma potential profiles in the plume of the BHT-200 are measured using a combination of electrostatic triple Langmuir probes and floating emissive probes. This article presents brief descriptions of the vacuum chamber, Hall thruster, and diagnostic techniques. The measured plasma properties are discussed in detail with particular emphasis on processes occurring along the thruster centerline. In particular, data believed to indicate the presence of collisionless shocks in the plume are presented along with theoretical justification for this hypothesis.

II. Experimental Apparatus

A. Thruster

The Busek BHT-200 Hall thruster serves as the test article for these experiments and is shown in Fig. 1, which also shows the coordinate system referred to throughout this article. An earlier version of this thruster is reported to operate at an anode efficiency of 42% and a specific impulse of 1300 seconds while providing 12.4 mN of thrust at the nominal operating conditions.[6] The thruster discharge channel has a mean diameter of 21 mm and is approximately 8 mm in width. A Busek 3.2-mm-diameter hollow cathode is used as an electron source for ionization of the xenon propellant and neutralization of the resulting plasma beam. The thruster is operated at nominal discharge conditions of 250 volts and 0.80 amps on anode and cathode propellant mass flow rates of 8.5 and 1.0 standard cubic centimeters per minute (sccm), respectively.

B. Vacuum Facility

All experiments discussed in this article are performed in Chamber 6 at AFRL. Chamber 6 is a 1.5 x 2.4 meter cylindrical, stainless steel vacuum chamber that is evacuated by four cryopanels maintained at 25 Kelvin by four APD cold heads, HC-8C helium compressors, and an APD cryopump.[7] This system provides a pumping speed of 26,000 liters per second on xenon with a base pressure of 3.2×10^{-7} Torr as measured by a

MKS Model 910 hot cathode gauge. During thruster operation, the pressure in the chamber rises to approximately 5.8×10^{-6} Torr corrected for xenon.

C. Triple Probe

The triple probes used for this experiment consist of three tungsten electrodes insulated from each other by an alumina rod. Two separate probes are used. For the larger probe, the diameter of each electrode is 0.50 mm (0.02") and the length extending past the end of the alumina is 5.0 mm (0.20"). A smaller probe consisting of 0.38 mm (0.015") diameter, 3.8 mm (0.15") long electrodes is used in areas of the plume where improved spatial resolution is desired. In each case, the spacing between the electrodes is approximately two electrode diameters. The probes are sized to criteria that allow the standard assumptions of probe theory to be applied.[8] These criteria are summarized in Eqns. 1-5 below and are necessary to ensure that all ions entering the probe sheath are collected by the probe rather than being deflected by magnetic fields or collisions. Further, it is assumed that the electrodes are far enough apart to avoid interaction with each other and that the spatial gradients of plasma properties are sufficiently small such that all three electrodes are exposed to identical plasmas. Additionally, the electron energy distribution is assumed to be Maxwellian. In the relations that follow, $r_{Li,e}$ are the ion and electron Larmor radii, respectively, r_p is the probe radius, λ_D, is the Debye length, dx depicts the distance between adjacent electrodes, and λ_c represents the total collision mean free path. The characteristic length scale over which plasma properties change significantly is denoted by Δ. The data collected in this experiment satisfy Eqns. 1-5

throughout most of the sampled volume. The areas where Eqn. 5 is not strictly satisfied are discussed in Section III.

$$r_{Li} >> r_{Le} >> \lambda_D \tag{1}$$

$$\lambda_D << r_p \tag{2}$$

$$\lambda_c >> r_p \tag{3}$$

$$dx >> \lambda_D \tag{4}$$

$$\Delta >> dx > r_p \tag{5}$$

The symmetric triple probe, originally developed by Chen and Sekiguchi,[9] is a convenient plasma diagnostic to use in Hall thruster plumes due to the elimination of the voltage sweep required by other electrostatic probes. Additionally, since the probe as a whole floats, the disturbance to the ambient plasma is minimized compared to single probes, which draw a net current from the discharge. A schematic of the triple probe circuit is shown in Fig. 2. In Fig. 2, electrode 2 is allowed to float while the voltage, V_{d3}, is applied by a laboratory power supply with floating outputs. For the tests reported here, V_{d3} was set to 12 volts. The probes are numbered in order of decreasing potential such that probe 2 is at the floating potential while probes 1 and 3 are biased above and below the floating potential, respectively.

The relations used to determine plasma properties from measured probe data are given in Eqns. 6-7. In these equations, n_e is the electron number density, which is equal to the ion number density through the quasineutrality assumption. The electron temperature is represented by T_e, and ion and electron masses are denoted by m_i and m_e, respectively. The symbol A denotes the area of a single electrode, e is the electron charge, and k_b is Boltzmann's constant. Various error analyses indicate that the uncertainty in the calculated electron temperature and number density are generally less than 30% and 50%, respectively.[9,10] The relative uncertainty between two data points recorded using the same probe is believed to be significantly lower than the absolute uncertainty.

$$n_e = \left(\frac{em_i}{k_b T_e}\right)^{1/2} \frac{I \exp\left(\frac{1}{2}\right)}{Ae^{3/2}\left[\exp\left(\frac{eV_{d2}}{k_b T_e}\right) - 1\right]} \tag{6}$$

$$\frac{1 - \exp\left(\frac{-eV_{d2}}{k_b T_e}\right)}{1 - \exp\left(\frac{-eV_{d3}}{k_b T_e}\right)} = \frac{1}{2} \tag{7}$$

D. Emissive Probe

Plasma potential measurements are conducted using a floating emissive probe similar to the one described by Haas *et al.*[11] The emitting portion of the probe consists of a loop of 0.127 mm (0.005") diameter tungsten filament, the ends of which are inserted into double bore alumina tubing along with 0.508 mm (0.020") diameter molybdenum

wire leads. Short lengths of tungsten wire are inserted into the alumina tube to insure contact between the emitting filament and molybdenum leads. The diameter of the emitting filament loop is approximately 3 mm. Fig. 3 shows a sketch of the emissive probe.

The theory of the emissive probe is well established and results in the conclusion that a thermionically emitting filament will assume the local plasma potential when its emitted electron current is sufficient to neutralize the plasma sheath.[12] For this experiment, the current necessary to heat the probe is provided by a programmable power supply with floating outputs. At each location in the plume, the current is steadily increased and the potential with respect to ground at the negative terminal of the power supply is recorded. This method allows for verification of a well-defined plateau in the voltage-current trace indicating neutralization of the plasma sheath. The shape of a typical trace, such as the one shown in Fig. 4, can be explained as follows. At zero applied current, the probe assumes the local floating potential. As the current to the probe is increased, the measured potential initially decreases as a voltage appears across the probe causing the potential at the negative terminal to move below the floating potential. As the probe current is increased further, the filament begins to emit electrons causing the measured potential to rise sharply before approaching an asymptote at the local plasma potential. Considering that the voltage drop across the emitting filament never exceeds 6 V, the uncertainty in the plasma potential measurements is estimated to be ±3 V.

III. Experimental Results and Analysis

A. Triple Probe

The larger triple probe is used to measure the electron number density and electron temperature at 5 mm intervals in the far-field Hall thruster plume. These data are taken in a plane perpendicular to the thruster face (the XZ plane in the coordinate system shown in Fig. 1) and are presented in Fig. 5 for axial locations 50-150 mm downstream of the thruster exit plane. Figure 5a shows a well-defined jet structure with a peak plasma density of approximately 1.5×10^{18} m^{-3} along the centerline of the thruster 50 mm downstream of the exit plane. The density falls off rapidly in both the downstream and transverse directions and is seen to decrease to less than 1.5×10^{17} m^{-3} just 150 mm downstream of the thruster. Note that the density contours in Fig. 5a are distributed exponentially rather than linearly for clarity. The electron temperature distribution, displayed in Fig. 5b, shows a similar structure to the plasma density plot with maximum temperatures occurring on centerline and decreasing in both the axial and transverse directions. The electron temperature varies between 1 and 2 eV over the majority of the displayed area and increases to nearly 3 eV along the thruster centerline at a distance of 50 mm.

In order to study the processes that occur along the centerline of the Hall thruster, measurements are taken in the near-field plume using both the large and small triple probe. The data presented in Fig. 6 are taken at 2 mm intervals using the larger probe.

Figure 7 shows measurements taken using the smaller probe at intervals of 1 mm in the X direction and 5 mm in the Z direction. These figures show several interesting features. The high density core seen in the far-field data is very pronounced in the near field data of Figs. 6a and 7a. Likewise, the high electron temperature core alluded to previously is the dominant feature of Figs. 6b and 7b. The most notable features shown in these plots are the unexpectedly high level to which the electron temperature rises along the thruster centerline and the relatively short distance (less than 10 mm) over which the increase occurs. Although the high density measured near the centerline is intuitive based on the picture of a radially converging plasma, there is no clear reason to expect the electron temperature to peak in this area. The regions where high plasma density and electron temperature are measured correspond to areas of the plume where a bright core is observed visually. This core is visible in Fig.8, which depicts four of the BHT-200-X3 thrusters during operation. The most likely explanations for these phenomena are discussed in Section IV.

Although the near-field data taken with the large and small probes show similar trends, there are several discrepancies that must be explained. In particular, the maximum values of both density and electron temperature recorded by the larger probe are significantly higher than those measured by the smaller probe. The most obvious explanation for this discrepancy is the significant level of uncertainty inherent in all electrostatic probe measurements. Indeed the difference in the peak densities recorded by the two probes falls within the 50% margin of error stated previously. The electron temperature profiles shown in Figs. 6b and 7b, on the other hand, show disagreement

well in excess of the 30% margin of error typical of triple probes. This leads to the conclusion that there is a source of error in the measurements taken near the thruster centerline that is not taken into account by the standard triple probe theory.

One of the most basic assumptions in the derivation of Eqns. 6-7 is that all three electrodes comprising the triple probe are exposed to identical plasmas.[9] Near the thruster centerline, the measured electron temperature and number density change over such a short distance that this assumption is not justified for this region of the plume. Figures 9a and 9b show normalized traces of the electron number density and electron temperature, respectively, measured at various locations downstream of the thruster face using the small probe. The data in each curve are normalized by the maximum value recorded at the given axial location. These traces show that both the electron temperature and number density appear to change by as much as 20% over a distance of just 1 mm near the thruster centerline at the upstream end of the sampled region. Considering that the electrodes of the small probe are separated by approximately 2 mm, it is clear that the identical plasma assumption is not satisfied near the thruster centerline. Similar traces taken using the larger triple probe (not shown) indicate changes of plasma properties in excess of 50% over the roughly 4 mm diameter of the probe. Clearly, errors caused by gradients in plasma parameters should be more pronounced in data taken using the larger probe. This leads to the belief that the smaller probe more accurately depicts the plasma properties near the centerline than the larger probe, although even these data are subject to a significant degree of uncertainty. The idea that the discrepancies shown in Figs. 6 and 7 are caused by failure of the identical plasmas assumption is enhanced by the fact

that both probes agree reasonably well in areas outside the central core. Differences in plasma properties between the two electrodes is also likely to be responsible for the asymmetry shown in the electron temperature data since the sign of the error would be reversed depending on which electrode, 1 or 3, is exposed to the higher density and electron temperature plasma. Although the absolute values measured in regions of high density and temperature gradients cannot be determined precisely, the data clearly indicate a significant rise in the electron temperature and electron number density near the thruster centerline.

B. Emissive Probe

Figure 10 shows plasma potential measurements taken in the XZ plane of the thruster at axial locations ranging from 50 to 150 mm downstream of the exit plane. These data are taken at 5 mm intervals in both the X and Z directions with the normal to the plane of the loop formed by the emitting filament oriented in the X direction. Like the density and electron temperature, the plasma potential is highest near the thruster centerline and falls off rapidly in the radial, or X, direction. At 50 mm downstream, the plasma potential peaks at approximately 20 volts along centerline and falls to less than 5 volts at the boundaries of the sampled region. By 150 mm downstream, the peak plasma potential decreases to less than 10 volts.

Near-field plasma potential measurements recorded 20 to 40 mm downstream of the thruster exit plane are presented in Fig. 11. Due to the high plasma density in this

region, the lifetime of the emitting filament is reduced compared to those used for far-field measurements and two separate probes are needed to collect the displayed data. The Z=20 traces are obtained with the first probe while the data at Z=30 and Z=40 are collected using a second identical probe. The plasma potential is seen to increase sharply near the thruster centerline, especially at short distances downstream of the thruster exit plane. The data taken 20 mm downstream, for example, show an increase of roughly 8 volts over a distance of approximately 2 mm. Assuming that this structure is axisymmetric, the physical size of the probe is again called into question. It should be noted that the diameter of the emitting filament loop is approximately 3 mm and hence is only marginally smaller than the width of the observed core. However, this does not qualitatively change the result that a region of high plasma potential appears along the thruster centerline and that the rise from the value in the surrounding plasma occurs over a very short distance. It does, on the other hand, imply that the apparent width of the core should be considered a rough approximation since slight misalignment of the probe in the Y direction could cause the core to appear narrower than it really is.

IV. Discussion

A. Two-Stream Instabilities

In an annular thruster, such as the BHT-200-X3, a portion of the accelerated ion beam converges along the thruster centerline. This creates a situation where the ion beam from one part of the thruster passes through its mirror image created in a diametrically opposed location. There are several instabilities that can be excited in a situation like

this, but before discussing them it is useful to consider some of the key plasma parameters in the plume so that these estimates can be used to determine which instabilities are expected to dominate. Table I presents several important parameters for a plasma with density, $n_e=5x10^{17}$ m^{-3} and electron temperature, $T_e=2$ eV, which are approximate values taken from the presented triple probe data. The ion drift velocity, V_{drift}, is estimated by assuming the ions are accelerated through a potential drop of 200 V.[5] The ion temperature, T_i, is assumed to be 1 eV, which is consistent with laser induced fluorescence (LIF) measurements obtained in the plume of a larger Hall thruster.[13,14] Measurements of the magnetic field obtained using an FW Bell Model 7030 gaussmeter and displayed in Fig. 12 show the field strength to be approximately 80 gauss along the thruster centerline at an axial distance of 10 mm. By 20 mm downstream the field strength falls to roughly 30 gauss and to less than 10 gauss at a distance of 50 mm. A value of 30 gauss is used to estimate the parameters given in Table I, which are intended only to show the scale of relevant parameters and are not necessarily quantitatively accurate. All quantities were calculated for xenon using approximate numerical formulas.[15]

In a situation where two unmagnetized ion components flow perpendicular to a magnetic field through a background of magnetized electrons there are at least six distinct instabilities that may exist.[16] These instabilities may be divided into two groups based on the frequency of the unstable waves. The higher-frequency "ion acoustic like instabilities" consist of the electron/ion acoustic (sometimes just called ion acoustic), the ion/ion acoustic (or ion/ion two-stream), and the electron cyclotron drift instabilities.[16]

The "lower hybrid like instabilities" occur at lower frequencies and include the ion/ion lower hybrid instability and two electron/ion modified two-stream instabilities that can occur between the background electrons and each ion component.[16] Of these two groups, the lower hybrid like instabilities are less likely to occur in the Hall thruster plume for several reasons. First, these instabilities produce a magnetized electron response to the fluctuating fields.[16] Although the electrons are weakly magnetized by the static fields downstream of the Hall thruster, no evidence suggesting the existence of large scale fluctuating fields has been observed. Additionally, all three of the low-frequency instabilities occur at wavelengths that are large compared to the electron Larmor radius (Table I).[16] This suggests that any effects due to this mode are likely to occur over length scales significantly larger than the structures seen in Figs. 7, 9, and 11.

Of the high-frequency modes, the first to consider is the electron/ion acoustic instability that can occur in current carrying plasmas. This mode is not likely to be significant in the present situation since it has been shown to require $T_e/T_i >> 1$, which is inconsistent with the estimates reflected in Table I.[17,18] Further, even if this mode becomes unstable, quasilinear theory shows that it generally only serves to flatten the slope of the electron velocity distribution function, df_e/dv, in a relatively narrow region of velocity space[19] and would not be expected to significantly alter macroscopic plasma parameters such as the electron temperature.

The electron cyclotron drift instability may play a crucial role along the centerline of a Hall thruster since it is the only high-frequency instability that persists for $T_e \approx T_i$.[16]

This instability occurs as a result of coupling between a Doppler-shifted ion acoustic mode and an electron cyclotron mode[20] and can cause significant heating of the electron component.[21] Additionally, since the unstable waves involved in this instability typically have wavelengths much shorter than the electron gyroradius,[22] this mode is likely to be important in the present situation where the distance over which interactions appear to occur is on the order of the gyroradius.

The final, and perhaps most important, instability to consider is the ion/ion acoustic instability. Given the estimate of $T_e/T_i \approx 2$ reflected in Table I, this mode appears to be stable since it has been shown to require $T_e/T_i >> 1$.[23] This may not be the case, however, when one considers the significant margin of error contained in both the electron and ion temperatures used in the estimate of the temperature ratio. The electron temperature has an estimated uncertainty of 30%, while the ion temperature estimate of 1 eV is taken simply as a typical value from the measured range of 0.4 to 2.0 eV.[13,14] Considering that numerical studies have shown the threshold value of the electron to ion temperature ratio to be approximately 3-4 for intersecting equidensity ion beams,[24] it is entirely possible that this criterion is met in the Hall thruster plume. Further, the electron cyclotron drift instability discussed above has been shown to be capable of causing electron heating over relatively short length scales. It is likely that this scenario could cause the electron to ion temperature ratio to increase to the threshold where the ion/ion mode becomes unstable. This phenomenon is demonstrated by the computer simulations of Schriver and Ashour-Abdalla where initially cold electrons in the Earth's plasma sheet

boundary layer are heated by electron/ion instabilities to the point where the ion/ion acoustic instability is excited.[25]

Assuming that the ion/ion acoustic instability is excited, it is expected to dominate the other modes discussed here since it has been shown to have the largest growth rate over a wide variety of parameters.[24] A final feature, which is relevant to the upcoming discussion, is the response of this instability to high flow speeds. As the ratio of the relative flow speed between the ion components to the ion thermal velocity is increased, the instability growth rate reaches a maximum and then returns to a stable condition for waves propagating parallel to the flow direction.[24, 26] As this happens, the direction of maximum wave growth shifts to successively steeper angles with respect to the flow.[27] This results in a condition where the instability propagates only at angles strongly oblique to the flow at high relative drift speeds.[24]

B. Collisionless Shocks

There are several reasons to suspect that collisionless shocks may occur in the plume of a Hall thruster. First, ion acoustic shocks have been proposed as an explanation for the well-defined boundaries of the bright core seen along the centerline of each thruster in Fig. 8.[6] Second, LIF measurements obtained by Smith *et al.* show a significant population of ions along the centerline of a Hall thruster having nearly zero radial velocity, but large axial velocity.[28] There is clearly no way for an ion originating in the annular discharge region of a Hall thruster to reach the centerline with zero radial

velocity unless it is deflected somehow. Since collisions are too rare to deflect a significant population into this region of velocity space, it is reasonable to hypothesize that the deflection mechanism may be a collisionless shock propagating obliquely to the flow direction. Finally, it has been well established, both analytically and experimentally, that the ion-ion two-stream instability discussed above can cause the dissipation necessary to form a collisionless shock.[29-33]

Judging by the magnetic field profiles shown in Fig. 12 and the orientation of the boundaries of the bright core seen in Fig. 8, any shock present in the system is likely to propagate perpendicular to the magnetic field and thus be based on magnetosonic waves.[34] Although it may seem counterintuitive to consider the role of the weak magnetic field downstream of a Hall thruster, Tidman and Krall have shown that magnetosonic waves are dominant over ion acoustic waves in low-beta plasmas such as the one described by Table I.[33] Further, since the magnetosonic shock degenerates into the ion acoustic shock when the magnetic field strength approaches zero,[34] it is possible to consider the former without losing information about the ion acoustic mode that occurs in this limit.

Across a magnetosonic shock, the magnetic field strength increases and an electric field exists that serves to decelerate the positively charged ions.[35] Interactions with this electric field are the source of the electron heating observed across the shock.[35-37] Rather than concentrate on the complexities of these physical mechanisms, however, it is sufficient for the purposes of this study to compare the results presented in Section III

to reported shock properties in an effort to determine if the existence of collisionless shocks in the thruster plume is consistent with the observed phenomena. To facilitate this effort, a simple model based solely on geometric arguments and observations of reported shocks is presented. This method cannot be expected to produce quantitatively accurate results, because it neglects potentially important effects such as the thermal spread of the ion distribution and the change in magnetic field strength across the shock. It does, however, illustrate several properties of the proposed shock. In particular, this model explains how a distinct jump in electron temperature and plasma potential can occur with only a modest rise in plasma density. The geometry and nomenclature used for this crude model are given in Fig. 13.

The model illustrated in Fig. 13 gives a rough estimate of the changes in plasma properties as a function of the shock divergence angle, α, the radial location in the exit plane where a sample ion is "born", r, and the downstream distance where that ion intersects the shock surface, d. The model depends on several limiting assumptions and geometric arguments, namely:

i.) The shock only affects the normal component of velocity such that, $V_{t1}=V_{t2}$, $V_{n1}>V_{n2}$.

ii.) The shock must turn the flow so that downstream of the discontinuity the flow is directed parallel to the thruster centerline.

iii.) Ions follow straight lines from the exit plane to the shock interface and are not subjected to collisions or external electric and magnetic fields.

iv.) At all points for which this model is applied, $r > d\sin(\alpha)$.

The assumptions listed above have several weaknesses. In particular, assumption ii) overstates the change in plasma flow because a shock needs only rearrange the velocity distribution such that the downstream distribution is stable. It does not necessarily turn all ions parallel to the centerline. Assumption iii) is not strictly accurate for a Hall thruster plume since it is widely acknowledged that a significant portion of the ion acceleration occurs downstream of the exit plane.[11] The cumulative effect of these weaknesses is to limit the range of parameters over which the model gives reasonable results. Specifically, this simple model is only valid for $d/r \geq 3$ such that the change in ion direction is not too large. Assumption iii) restricts the model to cases where the change in energy associated with the magnetic field is small compared to the change in kinetic and thermal energy across the shock. Using the assumptions mentioned above, it is possible to write the normal component of upstream and downstream ion velocity as given by Eqns. 8 and 9. These can be used to calculate the change in number density and velocity across the shock as given by Eqn. 10.

$$\frac{V_{n1}}{V_1} = \frac{\cos(\alpha)}{\sqrt{\left(1-\frac{d}{r}\tan(\alpha)\right)^2 + \left(\frac{d}{r}\right)^2}} \tag{8}$$

$$\frac{V_{n2}}{V_1} = \sin(\alpha)\left[\frac{\frac{d}{r}+\frac{d}{r}\tan^2(\alpha)-\tan(\alpha)}{\sqrt{\left(1-\frac{d}{r}\tan(\alpha)\right)^2 + \left(\frac{d}{r}\right)^2}}\right] \tag{9}$$

$$\frac{n_2}{n_1} = \frac{V_{n1}}{V_{n2}} = \frac{\cot(\alpha)}{\frac{d}{r} + \frac{d}{r}\tan^2(\alpha) - \tan(\alpha)} \tag{10}$$

$$\Delta\phi \cong \frac{m_i}{2e}\left(V_{n1}^2 - V_{n2}^2\right) \tag{11}$$

$$\Delta\left(\frac{k_B T_e}{e}\right) \cong \frac{\zeta m_i}{2e}\left(V_{n1}^2 - V_{n2}^2\right) \tag{12}$$

The electrostatic potential jump is, in general, dependent upon the frame in which it is measured.[35, 37] For the relatively weak shocks considered here, however, the frame dependence can be ignored and the potential jump can be estimated as the change in ion kinetic energy as given by Eqn. 11, where ϕ represents the plasma potential.[38,39] The electron temperature jump across a collisionless shock is shown empirically to be 5-20% of the incident flow ram energy.[36, 40] An estimate for the jump in electron temperature is given by Eqn. 12, where ζ is an empirical coefficient representing the fraction of dissipated ion kinetic energy that is converted to electron thermal energy.

Considering the discussion above, an increase in electron temperature without a pronounced jump in plasma density above that expected from radial convergence can be explained as being due to the large mass of a xenon ion. A small change in ion velocity causes an equally small change in number density, but a relatively large change in kinetic energy due to the large ion mass. As Eqns. 10 and 12 demonstrate, the change in number density depends only on the velocity change across the discontinuity while the electron

temperature also depends on the ion mass. Consequently, the change in electron temperature is quite noticeable because it is directly related to the kinetic energy lost by the ions rather than the density ratio across the shock, and therefore to relate the two quantities, it is necessary to assume an initial ion velocity. Figure 14 shows the electron temperature change for various values of ζ as a function of the density jump across a shock with α=10° for 200 volt xenon ions using the simple model. As this figure shows, significant changes in electron temperature can occur across a shock even for a relatively modest change in plasma density. For example, if one uses the crude model discussed above and considers a shock divergence half angle of 10°, as observed by Hruby *et al.*,[6] and an initial ion kinetic energy of 200 volts, the electron temperature change of roughly 2-3 eV shown between X=0 and X=10 mm in Fig. 7b corresponds to a density change of only about 50% for typical values of ζ.

V. Conclusions

The plasma properties in the plume of a low-power Hall thruster are measured using a combination of triple Langmuir probes and emissive probes. The results show unexpectedly high values of electron temperature and plasma potential in the high density regions along the thruster centerline. These properties occur in regions where a bright plasma core can be seen visually and are believed to be caused by collisionless shock waves. Such shocks can be induced as a result of the ion/ion acoustic two-stream instability that is likely to occur along the thruster centerline. Although further analysis and numerical simulations would be required to verify the development of a collisionless

shock for the conditions present in the thruster plume, a simple model has been presented showing the observed properties to be consistent with this hypothesis.

Vi. Acknowledgements

The authors wish to thank Dr. Mitat Birkan of the Air Force Office of Scientific Research for sponsoring this project. A portion of this work was performed under the auspices of AFOSR Grant F49620-02-1-0051.

1. R.A. Spores, G.G. Spanjers, M. Birkan, T.J. Lawrence, Proceedings of the 2001 AIAA Joint Propulsion Conference, AIAA Paper No. 2001-3225 (American Institute of Aeronautics and Astronautics, Washington, DC, 2001).
2. G.G. Spanjers, M. Birkan, and T.J. Lawrence, Proceedings of the 2000 AIAA Joint Propulsion Conference, AIAA Paper No. 2000-3146 (American Institute of Aeronautics and Astronautics, Washington, DC, 2000).
3. B.E. Beal, A.D. Gallimore, and W.A. Hargus, Proceedings of the 2002 AIAA Joint Propulsion Conference, AIAA Paper No. 2002-4251 (American Institute of Aeronautics and Astronautics, Washington, DC, 2002).
4. W. A. Hargus and G. Reed, Proceedings of the 2002 AIAA Joint Propulsion Conference, AIAA Paper No. 2002-3678 (American Institute of Aeronautics and Astronautics, Washington, DC, 2002).
5. B.E. Beal and A.D. Gallimore, Proceedings of the 2003 International Electric Propulsion Conference, IEPC Paper No. 2003-0035 (Electric Rocket Propulsion Society, Santa Fe, NM, 2001).
6. V. Hruby, J. Monheiser, B. Pote, P. Rostler, J. Kolencik, and C. Freeman, Proceedings of the 1999 AIAA Plasmadynamics and Lasers Conference, AIAA Paper No. 99-3534 (American Institute of Aeronautics and Astronautics, Washington, DC, 1999).
7. J.M. Haas, F.S. Gulczinski III, A.D. Gallimore, G.G. Spanjers, and R.A. Spores, Proceedings of the 1998 AIAA Joint Propulsion Conference, AIAA Paper No. 98-3503 (American Institute of Aeronautics and Astronautics, Washington, DC, 1998).

8. L. Schott, in Plasma Diagnostics, edited by W. Lochte-Holtgreven, (AIP Press, Woodbury, NY, 1995), Chap. 11, pp. 668-725.

9. S. Chen and T. Sekiguchi, J. Appl. Phys., **36**, 2363 (1965).

10. D.L. Tilley, A.J. Kelley, and R.G. Jahn, Proceedings of the 1990 International Electric Propulsion Conference, IEPC Paper No. 90-2667 (American Institute of Aeronautics and Astronautics, Washington, DC, 1990).

11. J.M. Haas and A.D. Gallimore, Phys. Plasmas, **8**, 652 (2002).

12. R.F. Kemp and J.M. Sellen, Jr., Rev. Sci. Instrum., **37**, 455 (1966).

13. G.J. Williams, Jr., T.B. Smith, F.S. Gulczinski, III, B.E. Beal, A.D. Gallimore, and R.P. Drake, Proceedings of the 1999 AIAA Joint Propulsion Conference, AIAA Paper No. 99-2424 (American Institute of Aeronautics and Astronautics, Washington, DC, 1999).

14. G.J. Williams, T.B. Smith, F.S. Gulczinski, and A.D. Gallimore, J. Prop. Power, **18**, 489 (2002).

15. J.D. Huba, NRL Plasma Formulary (Naval Research Laboratory, Washington, DC, 1998).

16. S.P. Gary, R.L. Tokar, and D. Winske, J. Geophys. Res., **92**, 10029 (1987).

17. B.D. Fried and R.W. Gould, Phys. Fluids, **4**, 139 (1961).

18. S.P. Gary and N. Omidi, J. Plasma Phys., **37**, 45 (1987).

19. R.J. Goldston and P.H. Rutherford, Introduction to Plasma Physics, (Institute of Physics Publishing, Philadelphia, PA, 1997), pp. 446-448.

20. H.V. Wong, Phys. Fluids, **13**, 757 (1970)

21. D.W. Forslund, R.L. Morse, and C.W. Nielson, Phys. Rev. Lett., **25**, 1266 (1970).

22. Y.M. Zhou, Y.Y. Li, and C.S. Wu, Phys. Fluids, **27**, 2049 (1984).

23. T.E. Stringer, Plasma Phys., **6**, 267 (1964).

24. S. P. Gary and N. Omidi, J. Plasma Phys., **37**, 45 (1987).

25. D. Schriver and M. Ashour-Abdalla, J. Geophys. Res., **95**, 3987 (1990).

26. B.D. Fried and A.Y. Wong, Phys. Fluids, **17**, 1048 (1974).

27. D.W. Forslund and C.R. Shonk, Phys. Rev. Lett., **25**, 281 (1970).

28. T.B. Smith, D.A. Herman, A.D. Gallimore, and R.P. Drake, Proceedings of the 2001 International Electric Propulsion Conference, IEPC Paper No. 01-0019 (Electric Rocket Propulsion Society, Columbus, OH, 1999).

29. C.F. McKee, Phys. Rev. Letters, **24**, 990 (1970).

30. R.J. Taylor, D.R. Baker, and H. Ikezi, Phys. Rev. Lett., **24**, 206 (1970).

31. D.W. Forslund and C.R. Shonk, Phys. Rev. Lett., **25**, 1699 (1970).

32. V.G. Eselevich and V.G. Fainshtein, Sov. J. Plasma Phys., **10**, 313 (1984).

33. D.A. Tidman and N.A. Krall, Shock Waves in Collisionless Plasmas (John Wiley & Sons, New York, NY, 1971).

34. N.A. Krall, Adv. Space Res., **20**, 715 (1997).

35. C.C. Goodrich and J.D. Scudder, J. Geophys. Res., **89**, 6654 (1984).

36. M. Gedalin, M. Balikhin, and V. Krasnosselskikh, Adv. Space Res., **15**, 225 (1995).

37. J.D. Scudder, Adv. Space Res., **15**, 181 (1995).

38. J.J. Sanderson, J. Appl. Phys. D, **9**, 2327 (1976).

39. D.L. Morse, Plasma Phys., **15**, 1262, (1973).

40. S.J. Schwartz, M.F. Thomsen, S.J. Bame, and J. Stansberry, J. Geophys. Res. **93**, 12923 (1988).

Table I: Estimated plasma properties in the near-field thruster plume.

Parameter	Approximate Value
Ion drift speed, V_{drift}, (m/s)	17,000
Ion thermal speed, v_i, (m/s)	850
Ion acoustic speed, C_s, (m/s)	1,500
Electron thermal speed, v_e, (m/s)	5.9×10^5
Alfven speed, C_A, (m/s)	8,000
Beta, $\beta = 8\pi n_e k_b T_e / B^2$	0.04
Electron Larmor radius, r_{Le}, (mm)	1.1
Electron plasma frequency (rad/s)	4.0×10^{10}
Electron cyclotron frequency (rad/s)	5.3×10^8
Electron Temperature, T_e, (eV)	2.0
Ion Temperature, T_i, (eV)	1.0

Figure 1: The BHT-200-X3 low-power Hall thruster and referenced coordinate system.

Figure 2: A schematic of the triple Langmuir probe circuit.

Figure 3: The floating emissive probe.

Figure 4: A sample emissive probe trace.

Figure 5: Electron number density (a) and electron temperature (b) measured in the far-field thruster plume using the large triple probe.

Figure 6: Near-field electron number density (a) and electron temperature (b) measured with the large triple probe.

Figure 7: Electron number density (a) and electron temperature (b) measured with the small triple probe. Note the lower temperatures shown here as compared to Figure 6b.

Figure 8: Four low-power thrusters in operation. Note the bright core along the centerline of each device.

Figure 9: Normalized electron density (a) and temperature (b) measured with the small triple probe. Note the short distances over which large changes occur.

Figure 10: The plasma potential measured in the far-field of the thruster plume.

Figure 11: Near-field emissive probe data showing a large increase in plasma potential near the thruster centerline.

Figure 12: The magnetic field downstream of the BHT-200-X3.

Figure 13: Simple shock model.

Figure 14: Electron temperature rise versus change in density across a shock for 200 volt ions using a simple geometric model.

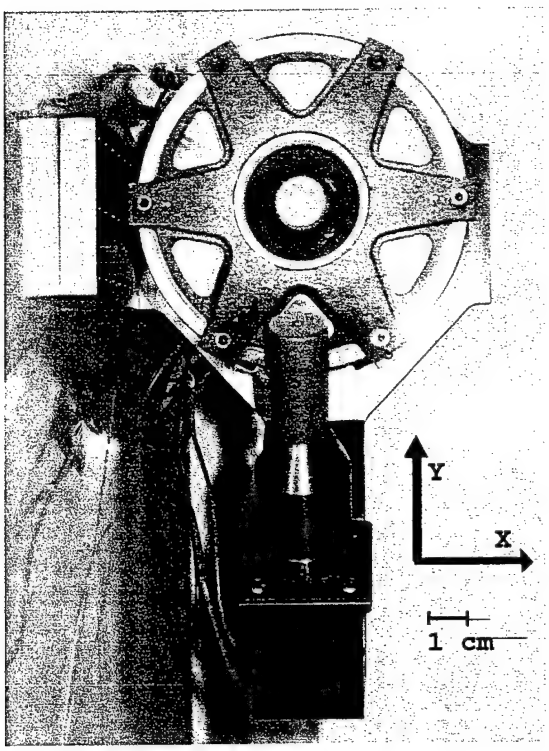

Figure 1, Beal, Physics of Plasmas

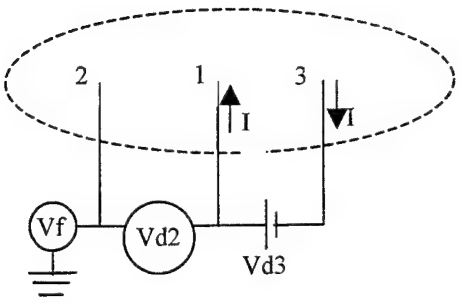

Figure 2, Beal, Physics of Plasmas

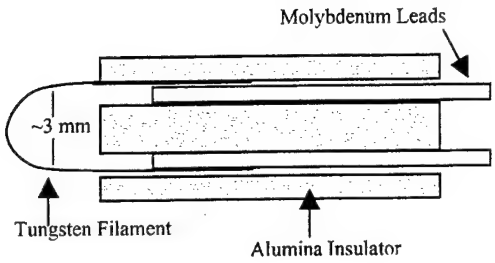

Figure 3, Beal, Physics of Plasmas

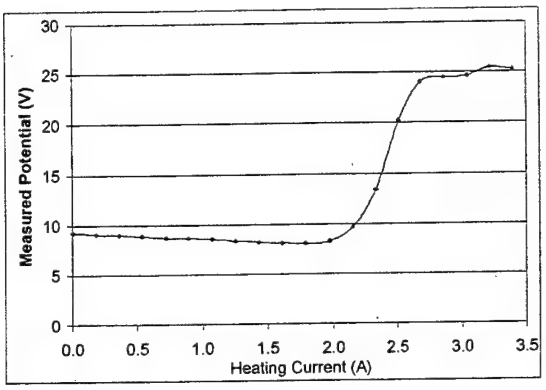

Figure 4, Beal, Physics of Plasmas

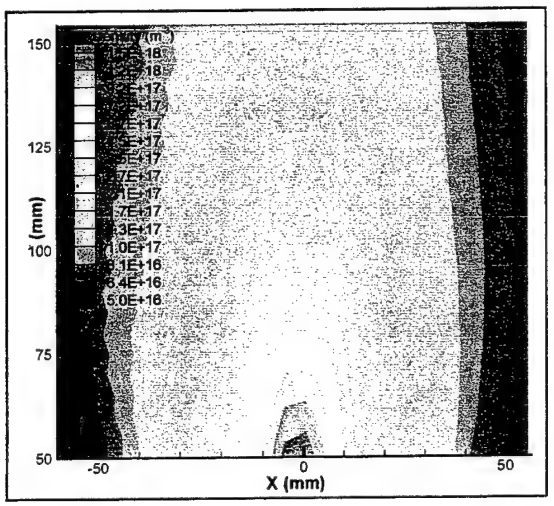

a.

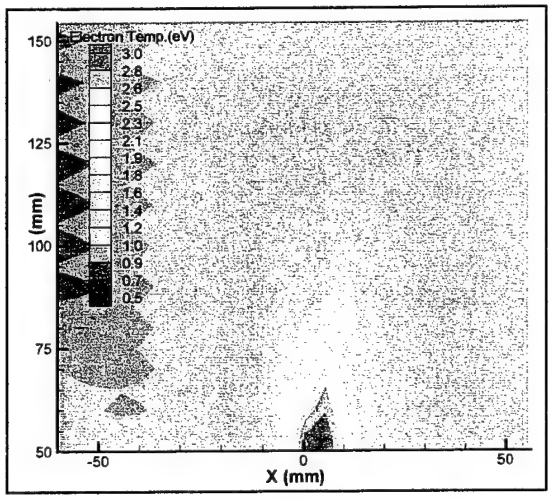

b.

Figure 5, Beal, Physics of Plasmas

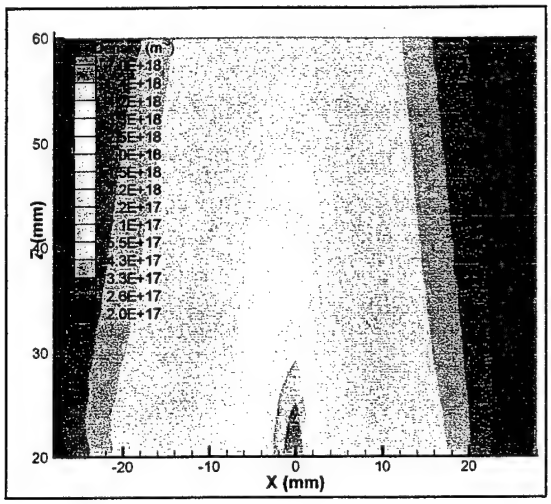

a.

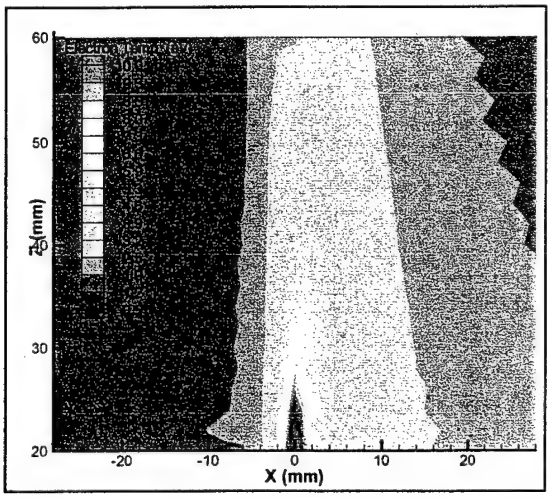

b.

Figure 6, Beal, Physics of Plasmas

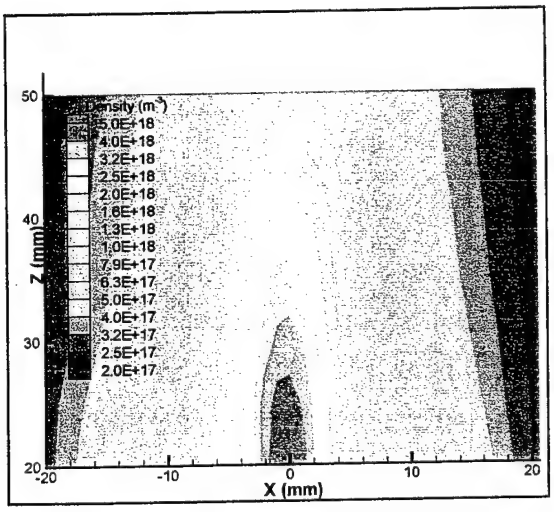

a.

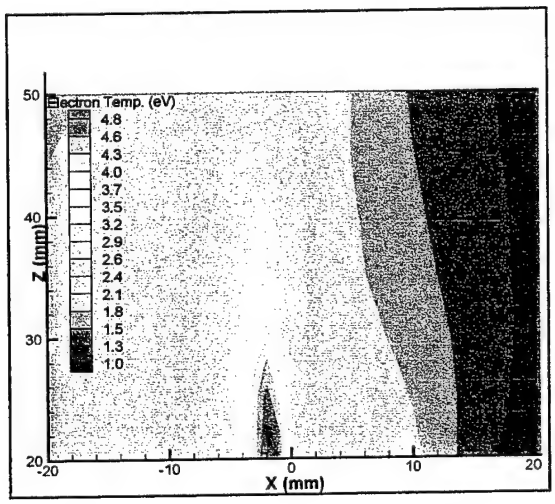

b.

Figure 7, Beal, Physics of Plasmas

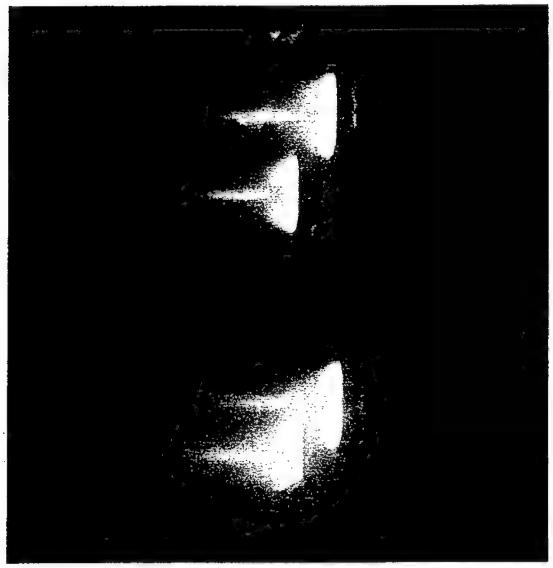

Figure 8, Beal, Physics of Plasmas

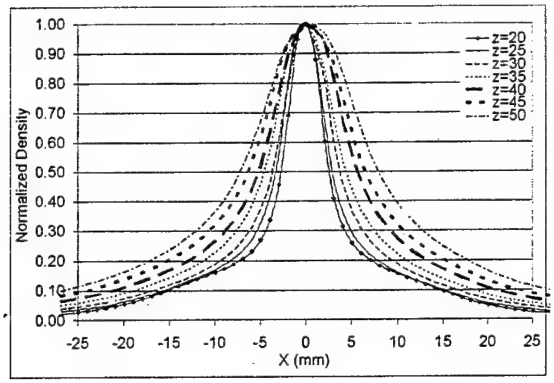

a.

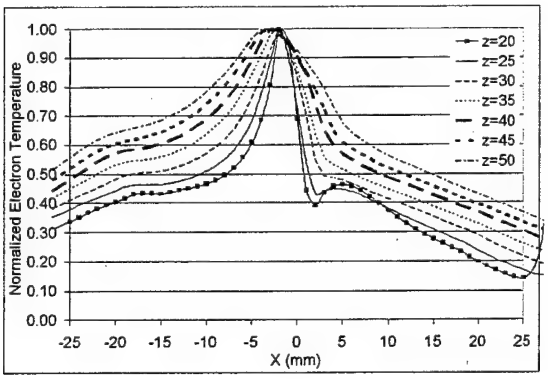

b.

Figure 9, Beal, Physics of Plasmas

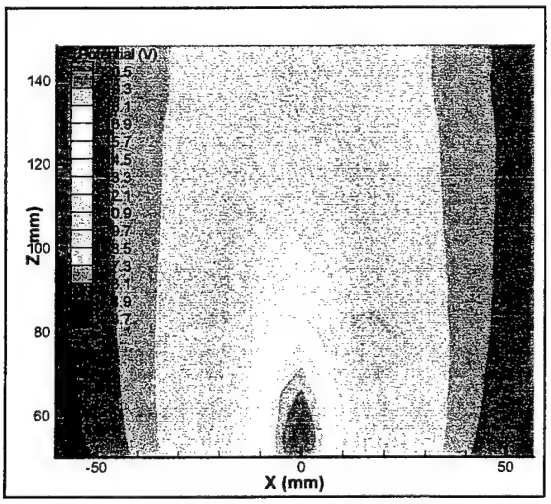

Figure 10, Beal, Physics of Plasmas

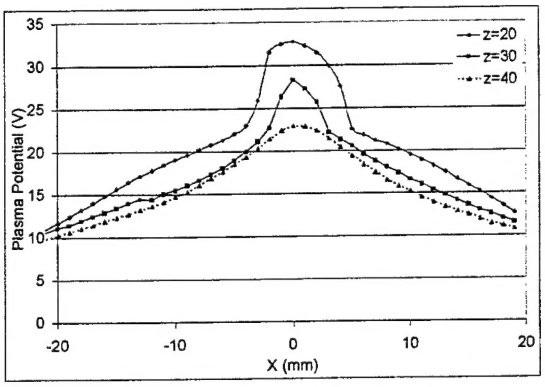

Figure 11, Beal, Physics of Plasmas

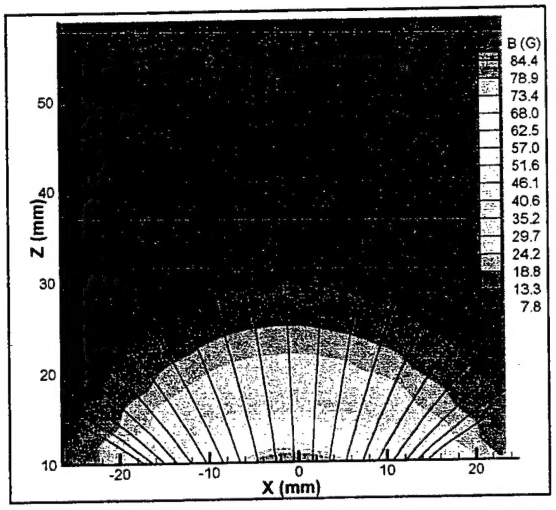

Beal, Figure 12, Physics of Plasmas

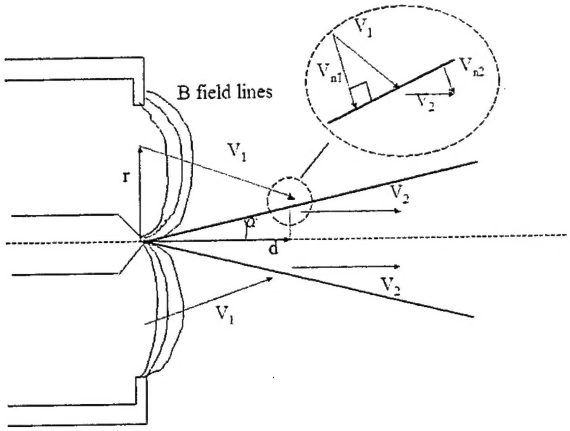

Beal, Figure 13, Physics of Plasmas

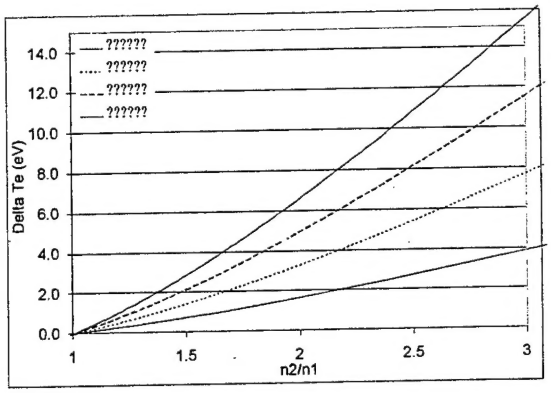

Beal, Figure 14, Physics of Plasmas